Effect of radiation losses on very lean methane/air flames propagating upward in a vertical tube

F.J. Higuera *, V. Muntean

E. T. S. Ingenieros Aeronáuticos, UPM, Plaza Cardenal Cisneros 3, 28040 Madrid, Spain

A B S T R A C T

2013

The stationary upward propagation of a very lean methane/air flame in a long vertical tube open at the bottom and closed at the top is simulated numerically using a single overall chemical reaction to model combustion and assuming an optically thin gas and a transparent or non-reflecting tube wall to approximately account for radiation losses from CO_2 and H_2O. Buoyancy plays a dominant role in the propagation of these flames and causes a large region of low velocity of the burnt gas relative to the flame to appear below the flame front when the equivalence ratio is decreased. The size of this region scales with the radius of the tube, and its presence enhances the effect of radiation losses, which would be otherwise negligible for a standard flammability tube, given the small concentration of radiating species. Heat conduction is found to be important in the low velocity region and to lead to a conduction flux from the flame to the burnt gas that causes extinction at the flame tip for a value of the equivalence ratio near the flammability limit experimentally measured in the standard tube. The effect of radiation losses decreases with the radius of the tube. Numerical results and order-of-magnitude estimates show that, in the absence of radiation, a very lean flame front fails to propagate only after recirculation of the burnt gas extends to its reaction region and drastically changes its structure. This condition is not realized for the standard flammability tube, but it seems to account for the flammability limit measured in a tube of about half the radius of the standard tube.

1. Introduction

Upward propagation of flame fronts in tubes filled with very lean reactive mixtures is a problem of both fundamental and applied interest which has been extensively studied. On the basis of a comprehensive analysis of previous work, Coward and Jones [1] proposed that a standard flammability tube can be used to characterize the flammability of gas mixtures. This is a vertical tube 51 mm in diameter and 1.8 m long with an open lower end and a closed upper end, which is filled with the mixture to be tested. This mixture is ignited near the lower end of the tube, and it is said to be flammable if a flame ensues and propagates all the way to the upper end. Levy [2] noted that buoyancy plays a dominant role in the propagation of the flame front near the flammability limit. This author observed that, when the Lewis number of the fuel is not far from unity, as in mixtures of methane/air or propane/air, the flame front consists of a spherical cap followed by a long skirt, and that its velocity is close to the velocity of a bubble rising in the tube [3]. The dependence of the flammability limit on the diameter of the tube was studied by Babkin et al. [4]. In agreement with some previous results but contrary to the results of Coward and Jones, these authors found that the minimum fuel concentration for which a flame front can propagate increases with the diameter of the tube. Lewis and von Elbe [5], Jarosinski et al. [6] and Hertzberg [7] pointed out that the stretch of the flame due to its curvature and to the strain rate of the flow it induces in the tube may cause the extinction observed at the flammability limit. Von Lavante and Strehlow [8] approximately computed the flow of the fresh gas above the flame front. They found that the stretch is due mainly to the strain rate of the flow; that it is of the order of the inverse of the residence time of the gas across a planar flame propagating in the mixture; and that it is maximum at the tip of the flame front, where extinction begins at the flammability limit. The flow on both sides of an axisymmetric steadily rising flame front was further investigated by Higuera [9], with emphasis on the structure of the vortical flow downstream of the flame front and the generation of vorticity at the flame. The results accurately determine the shape and stretch of the flame and point out a

possible instability of the vortical flow. Shoshin et al. [10] recently investigated the effect of preferential diffusion, which can increase the final combustion temperature of stretched flames when the Lewis number of the deficient reactant is smaller than unity. These authors, however, conclude that preferential diffusion cannot always explain the observed behavior of methane/air and propane/air flame fronts at their flammability limits. Shoshin and Jarosinski [11] and Shoshin et al. [12] proposed that heat losses from the flame due to the effect of radiation in a low velocity region that appears below very lean flames may explain the observed extinction.

Radiation losses in near limit flames propagating upward in a tube are further investigated in this paper. Numerical computations and order-of-magnitude estimations are used to show that the effect of these losses is very much enhanced by the conditions of the flow below the flame front. For very lean mixtures, this flow features a region of low velocity relative to the flame, whose radial extent scales with the diameter of the tube and whose length may be even larger. Heat conduction is important in this region, despite its large size, leading to a conduction heat flux from the reaction region of the flame to the burnt gas that is sufficiently strong to cause extinction of the flame in conditions typical of the standard flammability tube. This singular feature of the flow disappears, and radiation losses cease to play a role, when the equivalence ratio is slightly increased. The effect of the radiation losses also decreases with the radius of the tube. The reaction region at the tip of a very lean flame in a narrow tube is thick and tends to be located in a region of reverse (upward) flow, which may cause flame failure without radiation losses. Kinetic effects are important at the flammability limit. However, since analysis of these effects is beyond the scope of the present work, the combustion is modeled by means of a global irreversible Arrhenius reaction. This drastic simplification prevents any accurate analysis of flame extinction but, by keeping the computations affordable, it allows to clarify the mechanism by which low gas velocities and radiation losses act upon the flame.

2. Formulation

Consider an axisymmetric flame front rising at constant speed in a very long vertical tube of radius R^* whose wall is kept at a constant temperature T_u, as in the sketch of Fig. 1. The tube is open to the atmospheric pressure at its lower end and closed at its upper end, and it is filled with a very lean fuel-air mixture of density ρ_u, temperature T_u, and fuel mass fraction Y_u. A perfect gas with constant specific heats and mean molecular mass is assumed. Compressibility effects are left out by setting the pressure equal to a constant in the equation of state. The gas viscosity and thermal conductivity, μ and k, and the diffusivities of the fuel and the reaction products, D_i with $i = CH_4, CO_2, H_2O$ in the case of a methane flame, are taken to be powers of the temperature, of the form $\mu/\mu_u = k/k_u = \rho D_i/\rho_u D_{i_u} = (T/T_u)^\kappa$, so that the Prandtl and Lewis numbers, $Pr = \mu c_p/k$ and $Le_i = k/\rho c_p D_i$ respectively, are constant. Hereafter a subscript u denotes conditions in the fresh mixture. In what follows, $\kappa = 0.75$ and $Pr = Le_i = 1$ unless otherwise is noted. While more accurate molecular transport models are available for lean methane/air mixtures, such as the model developed by Smooke and Giovangigli [13], the simple power law model will suffice for the purposes of this work.

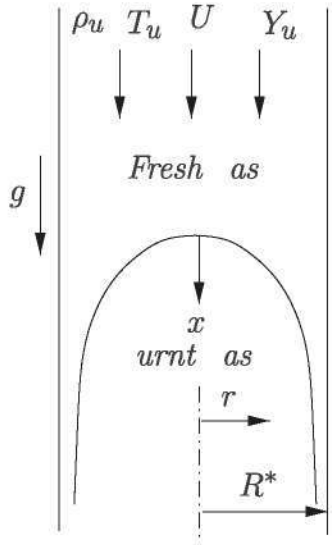

Fig. 1. Definition sketch. $R^* = 25.5$ mm for the standard flammability tube.

Combustion in the flame is modeled using a single irreversible Arrhenius reaction, $CH_4 + 2O_2 \rightarrow CO_2 + 2H_2O$ for methane/air, with frequency factor B and activation temperature T_a, so that the mass of fuel consumed per unit volume of gas and unit time is $w = \rho B Y_F \exp(-T_a/T)$, where ρ and T are the local gas density and temperature, and Y_F is the fuel mass fraction. Admittedly, a single-step chemistry is a poor model of the real kinetics. It cannot account for kinetic effects on flame extinction and does not allow to accurately determine the flammability limit. However, it is still useful to analyze the effects of gravity and thermal expansion, as well as the effects of preferential diffusion and radiation losses, which are the subject of this paper and seem to play an important role for near limit flames in the standard flammability tube.

The adiabatic flame temperature is $T_b = T_u + qY_u/c_p$, where q is the heat released per unit mass of fuel consumed. The dimensionless parameter $\gamma = (T_b - T_u)/T_u$ measures the thermal expansion of the gas in the flame, and the Zeldovich number $\beta = T_a(T_b - T_u)/T_b^2$ measures the temperature sensitivity of the chemical reaction. The equivalence ratio is $\phi = 17.39\,Y_u/(1 - Y_u)$ for methane/air mixtures. Well-known asymptotic analysis [14] shows that, in the limit $\beta \rightarrow \infty$, the velocity and thickness of a planar adiabatic flame are

$$U_L = \frac{(2D_b B)^{1/2} Le_F}{\beta(\gamma+1)} \exp\left(-\frac{\beta}{2}\frac{\gamma+1}{\gamma}\right) \quad \text{and} \quad \delta_L = \frac{k_u}{\rho_u U_L c_p}, \tag{1}$$

where $D_b = D_F(T_b)$ and Le_F are the diffusivity and the Lewis number of the fuel.

The values of the frequency factor and the activation temperature are chosen for the single-step chemistry to give planar flame velocities in agreement with experimental results in the range of equivalence ratios of interest. For this purpose, a reference case is considered (magnitudes denoted with a subscript r) where $T_u = 300$ K and $Y_{u_r} = 0.03$, so that $\phi_r = 0.538, T_{b_r} = 1500$ K and $\gamma_r = 4$ (using $c_p = 1287$ J/kg K), and the planar flame velocity is $U_{L_r} = 4.63$ cm/s according to Ref. [15]. For each value of the activation temperature T_a, the frequency factor B is chosen for the asymptotic formula (1) to reproduce this velocity in the reference case. The value $T_a = 18,750$ K, for which $\beta_r = 10$, is then determined for the flame velocity computed numerically with the single-step chemistry to fit the experimental results of Yamaoka and Tsuji [16] for very lean mixtures, corrected to zero stretch by Wang et al. [17]. This value of the activation temperature is in line with the results of Westbrook and Dryer [18]. Figure 2 shows the computed flame velocity (solid), the velocity given by the asymptotic formula (1) (dashed) and the experimental velocity (triangles) as functions of the equivalence ratio. Also shown in this figure are the planar flame velocities determined by Wang et al. [17] from their microgravity experiments (circles) and the fits obtained with the single-step chemistry for $T_a = 37,500$ K and 52,500 K (lower and upper dotted curves), though these values will not be used in what follows.

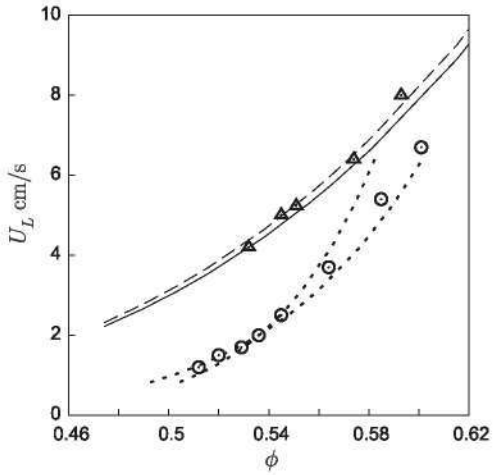

Fig. 2. Velocity of the planar flame as a function of the equivalence ratio. Triangles: experimental results of Yamaoka and Tsuji [16] corrected as in Ref. [17]. Solid: numerical results for single-step chemistry with $T_a = 18,750$ K. Dashed: asymptotic flame velocity (1) for this activation temperature. Circles: experimental results determined by Wang et al. [17] from their microgravity experiments. Dotted: numerical results for single step chemistry with $T_a = 37,500$ K (lower curve) and $T_a = 52,500$ K (upper curve).

Radiation from the reaction products CO_2 and H_2O is taken into account assuming that the gas is optically thin and the wall of the tube is transparent or non-reflecting. The energy lost by radiation per unit volume of gas and unit time is then $L = 4\sigma K_P T^4 - A$, where σ is the Stefan-Boltzmann constant, K_P is the Planck mean absorption coefficient, and A is the energy absorbed by the gas from the surrounding medium or the wall at temperature T_u; see, e.g., Ref. [19]. The coarse approximation $A = 4\sigma K_P T_u^4$, leading to $L = 4\sigma K_P \left(T^4 - T_u^4\right)$, will be used, which is admissible when T_u is small compared to the temperature of the radiating gas. The Planck mean absorption coefficient is written in the form $K_P = P_{CO_2} K_{CO_2} + P_{H_2O} K_{H_2O}$, where P_{CO_2} and P_{H_2O} are the partial pressures of CO_2 and H_2O, and K_{CO_2} and K_{H_2O} are functions of the gas temperature computed and tabulated by Ju et al. [20] using the statistical narrow band model; see also Fiveland [21] and Soufiani and Taine [22]. For the reference case, K_P is of the order of 1 m^{-1} in the burnt gas, where $P_{CO_2} \approx 0.054P$, $P_{H_2O} \approx 0.108P$, and $P \approx 10^5$ Pa is the total pressure of the gas. The absorption length K_P^{-1} is thus large compared to the radius of the tube ($R^* = 25.5$ mm for the standard flammability tube), which justifies the assumption of an optically thin gas.

An additional approximation will be used to simplify the computation of the radiation losses. Since the diffusivities of CO_2 and H_2O are not very different from each other, the approximation $Le_{CO_2} = Le_{H_2O}$ is made. This gives $P_{H_2O} = 2P_{CO_2}$, because the two species are produced and transported in the same conditions. Furthermore, since the mass fractions of these species are small for the lean mixtures considered, the approximation $P_{CO_2}/P \approx (Y_{CO_2}/44)/(0.23/32 + 0.77/28) = 0.655\,Y_P$ can be used, where Y_P is the mass fraction of CO_2. Thus, summarizing and using the equation of state of the gas, $L = 2.62\,\sigma R_g \rho Y_P T\left(K_{CO_2} + 2K_{H_2O}\right)\left(T^4 - T_u^4\right)$, where R_g is the constant of the air. To assess the effect of this approximation, computations have been carried out in which the mass fractions of CO_2 and H_2O are separately computed by solving the conservation equations for these species (analogous to Eq. (7) below) with $Le_{CO_2} = 1.39$ and $Le_{H_2O} = 0.83$. Some results are shown by dotted curves in Fig. 9 below. As can be seen, the approximation has only a small effect on the results. The factor $T\left(K_{CO_2} + 2K_{H_2O}\right)$ depends only weakly on the temperature and decreases when the temperature increases. Since most of the radiation losses occur from the hot burnt gas below the flame, where Y_P and $T^4 - T_u^4$ are largest, this factor is replaced by a constant equal to its value 0.25 K/Pa m at $T = 1300$ K. Again, additional computations in which the temperature variation of $T\left(K_{CO_2} + 2K_{H_2O}\right)$ is retained show that this approximation has no important effect on the results.

In most cases of interest, the wall of the tube is not transparent to the visible and infrared radiation emitted by the burnt gas. The wall absorbs and reflects this radiation partially (for Plexiglas, Pyrex or quartz tubes) or totally (for black or metallic tubes), and thus plays a role in the radiation exchange. The effect depends on the wall thickness and the optical and thermal properties of the tube material, and its analysis is beyond the scope of this work. The simple model of an optically thin gas enclosed by a transparent or non-reflecting wall is intended to give qualitative results only. Its use relies on the following estimations.

First, a coarse, conservative estimate of the temperature increase of the wall in a region of characteristic size R^* around the flame tip due to the absorbed radiation, ΔT_{wr} say, can be worked out assuming that all the radiation emitted by the burnt gas in this region, of order LR^{*3} with L evaluated at temperature T_b, is absorbed by the wall, and leaving out heat losses from the outer surface of the tube. In a reference frame moving with the flame front, in which the wall is seen to move downward with a velocity U_0 (see Fig. 1), an order-of-magnitude energy balance for the heated layer of the wall reads $\rho_s c_s U_0 R^* b \Delta T_{wr} \sim LR^{*3}$, where ρ_s and c_s are the density and specific heat of the tube material and b is the thickness of the heated layer; $b \sim \min(d_w, \sqrt{k_s R^*/\rho_s c_s U_0})$, with d_w denoting the thickness of the wall and k_s its thermal conductivity. Thus $\Delta T_{wr}/T_u \sim (\sigma K_P T_b^4 R^{*2})/(\rho_s c_s U_0 b T_u)$, which should be small for the cold wall condition used in this work to be realistic. For a standard tube ($R^* = 25.5$ mm) with the thermal properties of Plexiglas, taking $U_0 = 21$ cm/s (see Section 3 below) and $b = \sqrt{k_s R^*/\rho_s c_s U_0} = 0.11$ mm, the estimate gives $\Delta T_{wr}/T_u \sim 1.5 \times 10^{-2}$ in the conditions of the reference case mentioned above. Similarly, $\Delta T_{wr}/T_u \sim 5.6 \times 10^{-3}$ for a quartz tube, and 3.84×10^{-4} for an aluminum tube (with d_w larger than about 3 mm). The estimate of ΔT_{wr} is for a region of characteristic size R^* moving with the flame tip. The radiation-induced wall temperature increase may be larger than ΔT_{wr} far downstream of the flame tip, but this is not expected to significantly affect the propagation of the flame. Radiative heating of the wall far upstream of the flame tip is assumed to be small because the angle subtended by the burnt gas is then small.

Second, the reflection of gas-emitted radiation in the tube wall increases the intensity of the radiation in the tube and thus leads to an increase of gas absorption (A above) and a decrease of the net radiation losses, L. However, analysis of a hot isothermal gas enclosed by a cold wall [19] suggests that, for the optically thin gas envisaged here, the relative decrease of radiation losses due to multiple reflections is of order $K_P R^*/(1 - \rho_w)$, where ρ_w is the reflectivity of the wall. Since $K_P R^*$ is small, the decrease of the radiation losses is significant only for a nearly perfectly reflecting wall, with ρ_w close to unity. The effect approximately amounts to reducing the Planck mean absorption coefficient.

Dimensionless variables are now introduced. The values of the planar flame velocity and thickness given by the asymptotic formulae (1) for the reference case, namely $U_{L_r} = 4.63$ cm/s and $\delta_{L_r} = 0.43$ mm, will be used as units of velocity and length. When Y_u is changed keeping T_u constant, the parameters γ, β and U_L change as

$$\left.\begin{aligned} &\frac{\gamma}{\gamma_r} = \frac{Y_u}{Y_{u_r}}, \quad \frac{\beta}{\beta_r} = \frac{\gamma}{\gamma_r}\left(\frac{\gamma_r+1}{\gamma+1}\right)^2, \\ &U_f = \frac{U_L}{U_{L_r}} = \left(\frac{\gamma+1}{\gamma_r+1}\right)^{(\kappa+3)/2} \frac{\gamma_r}{\gamma} \exp\left[-\frac{\beta}{2}\frac{\gamma+1}{\gamma_r+1}\left(1 - \frac{\gamma_r}{\gamma}\right)\right], \end{aligned}\right\} \tag{2}$$

which give a γ proportional to Y_u; a β that decreases when Y_u increases in the range of values of interest (above $\gamma = 1$); and a U_f that increases rapidly with Y_u. In addition, the density is scaled with ρ_u, the mass fractions of all the species are scaled with Y_u, and the dimensionless temperature $\theta = (T - T_u)/(T_b - T_u)$ is used. In terms of these variables, the governing equations and boundary conditions in the reference frame moving with the flame front, in which the solution is stationary, are

$$\nabla \cdot (\rho \boldsymbol{v}) = 0, \tag{3}$$

$$\rho \boldsymbol{v} \cdot \nabla \boldsymbol{v} = -\nabla p + \rho G \boldsymbol{i} + \nabla \cdot \tau', \tag{4}$$

$$\rho \boldsymbol{v} \cdot \nabla \theta = \nabla(\lambda \nabla \theta) + W - L, \tag{5}$$

$$\rho \boldsymbol{v} \cdot \nabla Y_F = \frac{1}{Le_F} \nabla(\lambda \nabla Y_F) - W, \tag{6}$$

$$\rho \boldsymbol{v} \cdot \nabla Y_P = \frac{1}{Le_P} \nabla(\lambda \nabla Y_P) + \frac{11}{4} W, \tag{7}$$

$$W = \frac{\beta^2 U_f^2}{2(\gamma+1)^{\kappa-1} Le_F} \rho Y_F \exp\left[\beta(\gamma+1)\frac{\theta-1}{1+\gamma\theta}\right], \tag{8}$$

$$L = \rho \Sigma Y_P \left[(1+\gamma\theta)^4 - 1\right], \tag{9}$$

$$\rho(1+\gamma\theta) = 1, \quad \lambda = (1+\gamma\theta)^{\kappa}, \tag{10}$$

$$r = R: \quad \boldsymbol{v} = U_0 \boldsymbol{i},\ \theta = \frac{\partial Y_F}{\partial r} = \frac{\partial Y_P}{\partial r} = 0, \tag{11}$$

$$x \to -\infty: \quad \boldsymbol{v} = U_0 \boldsymbol{i},\ \theta = 0,\ Y_F = 1,\ Y_P = 0, \tag{12}$$

$$x \to \infty: \quad \frac{\partial \boldsymbol{v}}{\partial x} = \frac{\partial \theta}{\partial x} = \frac{\partial Y_F}{\partial x} = \frac{\partial Y_P}{\partial x} = 0, \tag{13}$$

where dimensionless variables are denoted with the same symbols used before for their dimensional counterparts. Here r is the dimensionless distance from the axis of the tube and x is the dimensionless distance along the axis measured downward from an origin which is defined by the condition that $\theta_0 = \theta(0,0)$ have a chosen constant value, typically 0.7 or 0.8; $\boldsymbol{i}$ is a unit vector pointing downward; and U_0 is the dimensionless velocity of the flame front relative to the tube, which is to be found as part of the solution. Eqs. (3) and (4) are the continuity and momentum equations, where $G = g\delta_{Lr}/U_{Lr}^2$ is the dimensionless acceleration of gravity, $\tau\prime = \lambda\left[\nabla \boldsymbol{v} + (\nabla \boldsymbol{v})^T\right]$ is the non-spherical part of the viscous stress tensor, and p is the pressure of the gas augmented with the spherical part of the viscous stress tensor, both scaled with $\rho_u U_{Lr}^2$. Eqs. (5)–(7) are the energy, fuel, and product (CO_2) conservation equations, with the reaction and radiation terms given by Eqs. (8) and (9). Eqs. (10) are the equation of state and the equation giving the power law temperature dependence of the dimensionless viscosity, conductivity and mass diffusivities. The boundary conditions (11)–(13), express that the wall of the tube and the fresh gas are seen to move downward with velocity U_0 in the reference frame tied to the flame front. Here $R = R^*/\delta_{Lr}$ is the dimensionless radius of the tube.

The dimensionless parameters appearing in (3)–(13) are

$$\left.\begin{aligned} &\gamma = \tfrac{T_b - T_u}{T_u}, \quad \beta = \tfrac{T_u(T_b - T_u)}{T_b^2}, \quad U_f = \tfrac{U_L}{U_{Lr}}, \\ &G = \tfrac{g\delta_{Lr}}{U_{Lr}}, \quad R = \tfrac{R^*}{\delta_{Lr}}, \quad Le_F, \quad Le_P, \quad Pr, \quad \kappa, \\ &\Sigma = 2.62\, \tfrac{\sigma R_g T_u^3 \delta_{Lr} Y_{u_r}}{c_p \gamma_r U_{Lr}} \left[T\left(K_{CO_2} + 2K_{H_2O}\right)\right]_{1300\ \mathrm{K}}. \end{aligned}\right\} \tag{14}$$

The first three parameters are given by (2) in terms of γ_r, β_r and Y_u/Y_{u_r}. Parameter U_f is artificial. It appears due to the use of U_{Lr} and δ_{Lr} as velocity and length scales instead of the values U_L and δ_L given by (1) for the current composition of the fresh gas. The magnitudes U_{Lr} and δ_{Lr} of the reference case are used for convenience, to facilitate comparison of results for mixtures with different fuel mass fractions in the same tube and setup. Since these magnitudes appear in most of the dimensionless parameters, all these parameters would change when Y_u is changed, should U_L and δ_L have been used in their definitions. Values of the dimensionless parameters used in the computations of the following section are $\gamma_r = 4, \beta_r = 10, Le_P = Pr = 1$ and $\kappa = 0.75$, as mentioned above; $Le_F = 0.8$, 1 and 1.2; $G = 2$ corresponding to normal gravity; $R = 60$ corresponding approximately to the standard flammability tube; and $\Sigma \approx 2 \times 10^{-5}$.

The numerical method used to solve (3)–(13) is similar to the method used in Ref. [9]. The stream function/vorticity formulation equivalent to (3) and (4) is used together with a pseudo-transient iteration which amounts to adding time derivatives to Eqs. (5)–(7) and the vorticity equation that results from (4). The equations are then rewritten in terms of the new independent variables (ξ, r), where $\xi = (x + vR)/(h(r) + vR)$, v is an adjustable constant, $h(0) = 0$, and the function $h(r)$ and the constant U_0 in (11) and (12) are iteratively chosen to ensure that $\theta(\xi = 1, r) = \theta_0$ in a region around the axis of the tube. The equations are discretized using second order finite differences in a rectangular, nonuniform grid covering the domain $[0, \xi_\infty] \times [0, R]$ and finer around $\xi = 1$. Typical values of the numerical parameters are $v = 1$ and $\xi_\infty = 3$–6. Numerical tests show that grid independence is obtained with 360×120 grid points.

3. Results and discussion

In agreement with experimental results and previous numerical computations [9,10], the flame fronts computed for very lean mixtures consist of a round cap followed by a long skirt; see, e.g. Figs. 3, 6 and 7 below. The shape of the cap is similar to that of a bubble rising in the tube, and its velocity U_0 is nearly independent of the equivalence ratio and close to the velocity of a bubble given by the Davies and Taylor formula [3],

$$U_{DT} = 0.467 \left(\frac{\gamma}{\gamma+1} GR\right)^{1/2} \tag{15}$$

in our dimensionless variables. Eq. (15) gives $U_{DT} = 4.58$ (which amounts to 21 cm/s) for $\gamma = 4, G = 2$ and $R = 60$. Since U_{DT} is scaled with U_{Lr}, this relatively large value implies that the tip of the flame front is confined to a neighborhood of the stagnation point of the equivalent bubble flow, and the rest of the flame front lies near the streamline through this point. Also, insofar as the dimensionless burning velocity of the flame is of the order of U_f in Eq. (2), the length of the skirt scaled with the radius of the tube is large of the order of U_{DT}/U_f.

3.1. Results without radiation losses

Consider first a flame front propagating upward in the absence of radiation losses ($\Sigma = 0$). Figure 3 shows the reaction region, some isotherms, and some streamlines of the flow relative to the flame for $Le_F = 1, R = 60$, and equivalence ratios ϕ = 0.344, 0.504, 0.538 and 0.581, which correspond to U_f = 0.07, 0.7, 1 and 1.5. Figure 4(a) summarizes some properties of the flame at its tip. Measuring vertical distances from the point where the reaction rate attains its maximum on the symmetry axis, x_W where $W = W_{max}$ say, this figure shows, as functions of ϕ, the distances from this point to the points where $W = 0.1\, W_{max}$ on either side of the maximum (solid lines), the distance to the point where $\theta = 0.1$ (dashed), and the distance to the point where $\boldsymbol{v} = 0$ (dotted) when such point, which marks the upper boundary of a recirculation region, exists (in Fig. 3(a) and (b), for example). Results are shown for $R = 60$ and Le_F = 0.8, 1 and 1.2, increasing as indicated by the arrows. Figure 4(b), to be commented below, shows similar results when radiation losses are taken into account with $\Sigma = 2 \times 10^{-5}$. The distance between the two solid curves in Fig. 4 is a measure

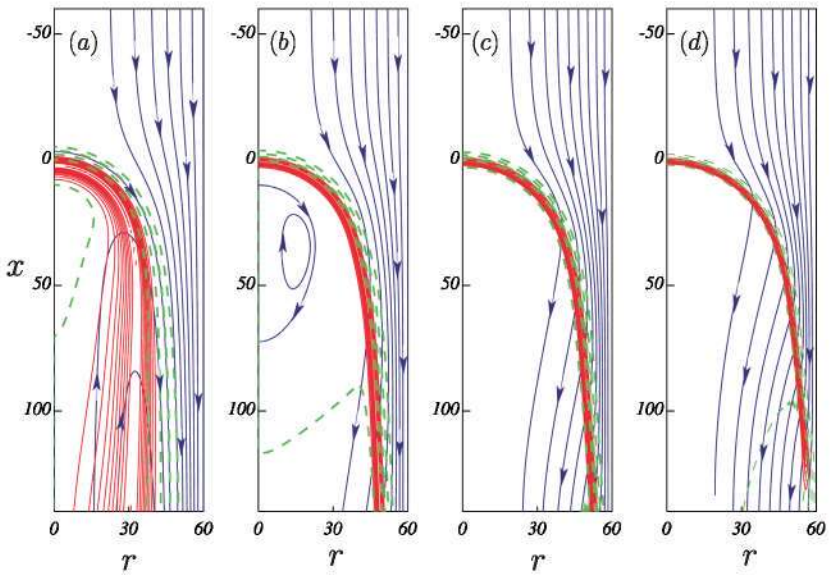

Fig. 3. Contours of constant reaction rate (W, solid, red), isotherms (dashed, green) and streamlines of the flow relative to the flame front (solid with arrows, blue) for $\phi = 0.344$ (a), 0.504 (b), 0.538 (c) and 0.581 (d), in the absence of radiation losses ($\Sigma = 0$). Other parameters have their reference values mentioned below Eq. (14). In particular, $G = 2, R = 60$ and $Le_F = Pr = 1$. (For interpretation of the references to color in this figure legend, the reader is referred to the web version of this article.)

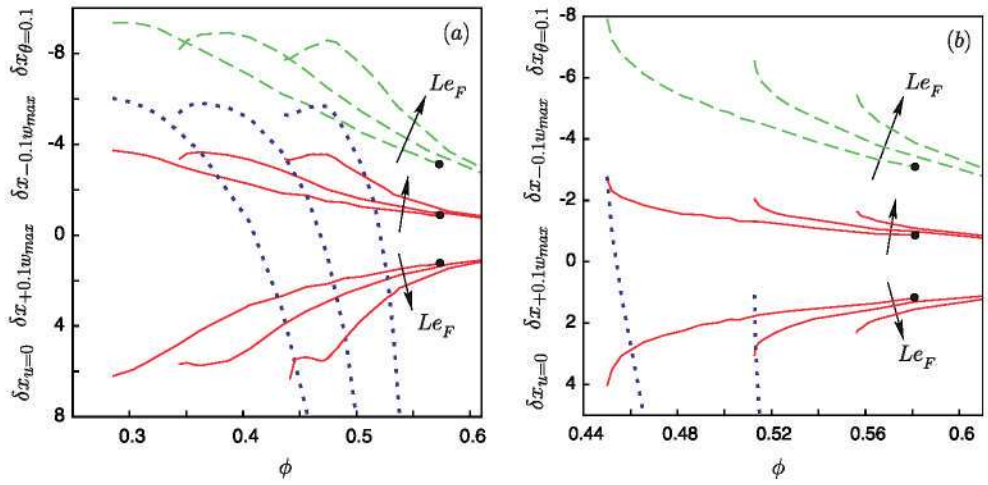

Fig. 4. Properties of the flame along the axis of the tube as functions of the equivalence ratio. Shown are the distances from the point where W attains its maximum (W_{max}) to the points where $W = 0.1\,W_{max}$ on both sides of the maximum ($\delta x_{\pm 0.1 w_{max}}$, solid red), to the point where $\theta = 0.1$ ($\delta x_{\theta=0.1}$, dashed, green), and to the stagnation point where $v = 0$ ($\delta x_{u=0}$, dotted, blue), for $Le_F = 0.8$, 1 and 1.2, increasing as indicated by the arrows. $\Sigma = 0$ in (a) and 2×10^{-5} in (b). Other parameters have their reference values. (For interpretation of the references to color in this figure legend, the reader is referred to the web version of this article.)

of the thickness of the reaction region, and the distance between the lower solid curve and the dashed curve is a measure of the thickness of the whole flame at the tip. When $Le_F = 0.8$, the flame transitions from bubble-shaped to tulip-shaped at the right-hand side end of the curves, for $\phi \approx 0.573$. Similar transitions occur for $Le_F = 1$ and 1.2 at higher values of ϕ, not shown in the figure.

As can be seen in Figs. 3 and 4(a), the following sequence of events occurs when the flame is weakened by decreasing the equivalence ratio. The downward velocity of the burnt gas relative to the flame front decreases around the axis of the tube (the spacing of the streamlines increases); a recirculation region appears below the flame front; the reaction region of the flame thickens and approaches the recirculation region; the reaction region enters the recirculation region; the numerical method ceases to converge to a stationary solution. When the Lewis number of the fuel is larger than unity, the strain rate of the flow ahead of the flame weakens it at the tip (see, e.g. Williams [14]) and the sequence of events occurs earlier, for larger values of the equivalence ratio than when $Le_F = 1$. Similarly, the strain rate strengthens the flame and postpones the sequence of events to smaller values of the equivalence ratio when $Le_F < 1$.

The structure of the flame changes significantly when most of the chemical reaction occurs in the recirculation region. The convection, conduction and reaction terms of the energy equation (5) along the axis of the tube are shown in Fig. 5 for $\phi = 0.406$ and 0.504. Convection is not important in the reaction region when $\phi = 0.504$, in which case the gas moves downward across the flame, but it is of the same order as the conduction and reaction terms when $\phi = 0.406$, and even larger than the reaction term when $\phi = 0.344$ (not displayed), in which cases the gas flows upward in the reaction region. This flow tends to confine the fuel that enters the recirculation region from above by diffusion across the dividing streamline bounding this region.

The increasing relative importance of convection when ϕ decreases can be explained using simple order-of-magnitude estimates. The Zeldovich number β is fairly large, implying that

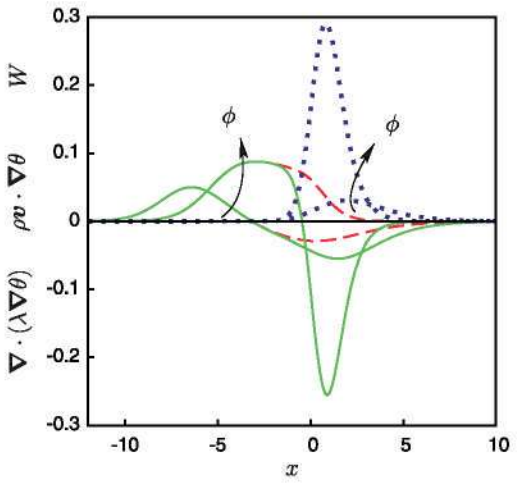

Fig. 5. Convection (dashed, red), conduction (solid, green) and reaction (dotted, blue) terms of the energy equation (5) along the axis of the tube for $\phi = 0.406$ and 0.504, increasing as indicated by the arrows. Here $\Sigma = 0$ and other parameters have their reference values. (For interpretation of the references to color in this figure legend, the reader is referred to the web version of this article.)

the dimensionless fuel mass fraction and the temperature variation are small in the reaction region, $(Y_F, 1-\theta) = O(\beta^{-1})$. The balance of conduction and chemical reaction, $\mathbf{\nabla}\cdot(\lambda\mathbf{\nabla}\theta) \sim W$, reads $\lambda_b\beta^{-1}/\delta^2 \sim W_c$, as for a planar unstretched flame [14]. Here δ is the characteristic thickness of the reaction region, $\lambda_b = (\gamma+1)^{\kappa}$, and $W_c = \beta U_f^2/(\gamma+1)^{\kappa}$, from (8) with $Y_F = O(\beta^{-1})$. The upward velocity of the gas in the reaction region is induced by the viscous shear stress at the dividing streamline, and depends on the conditions of the flow in the whole recirculation region. Denoting by u_c the order of this velocity, the ratio of convection to conduction terms of the energy equation in the reaction region is

$$\frac{O[\rho\boldsymbol{v}\cdot\mathbf{\nabla}\theta]}{O[\mathbf{\nabla}\cdot(\lambda\mathbf{\nabla}\theta)]} \sim \frac{\rho_b u_c \delta}{\lambda_b} \sim \frac{\rho_b u_c}{(\beta\lambda_b W_c)^{1/2}},$$

where $\rho_b = 1/(\gamma+1)$ and the estimate of δ above $[\delta \sim (\lambda_b/\beta W_c)^{1/2}]$ has been used. This ratio increases when W_c is decreased by decreasing ϕ, which suggests that convection would eventually overcome conduction. However, a convection–reaction balance does not make sense when the reaction occurs in the region of reverse flow, because this flow does not bring any fuel to the reaction region. Therefore a stationary flame is expected to fail at its tip when the ratio of convection to conduction reaches a certain limit value of order unity, which amounts to $U_{f_{lim}} \sim u_c/\beta(\gamma+1)$ when the estimate of W_c above is used (but see comments below for $Le_F \geqslant 1$).

This coarse estimation depends on the characteristic velocity of the gas u_c, which in turns depends on a number of factors. When the flow in the recirculation region is stationary, as in the computations of this paper, the balance of viscous shear stresses at the two sides of the dividing streamline (accounting for the increased viscosity of the burnt gas) suggests that the velocity in the bulk of the recirculation region should scale as $u_d = (GR)^{1/2}/(\gamma+1)^{\kappa}$, though the numerical results show that the actual velocity is somewhat smaller than this u_d. If the thickness of the reaction region is small compared to the radial extent of the recirculation region, $\delta \ll R$, then the reaction region is near the upper stagnation point of the recirculating flow and the estimate $u_c = u_d\delta/R$ is appropriate, which gives $U_{f_{lim}} \sim (G/R)^{1/4}/\beta(\gamma+1)^{1/2}$. If the condition $\delta \ll R$ is not satisfied, as in the results for $R = 30$ displayed in Fig. 6(a), then $u_c = u_d$ is appropriate, which gives $U_{f_{lim}} \sim (GR)^{1/2}/\ \beta(\gamma+1)^{1+\kappa}$. As can be seen, the two estimates of u_c predict opposite trends for the limit value of U_f (hence ϕ_{lim}) as a function of the radius of the tube. The first prediction is analogous to the results derived on the assumption that flame stretch due to the strain rate of the fresh gas flow causes extinction at the flammability limit (e.g., Buckmaster and Mikolaitis [23]). The second prediction is similar to the prediction put forward by Levy [2].

A region of distributed reaction exists away from the tip of near limit flames when $Le_F \geqslant 1$; see, e.g., Fig. 3(a). In these cases, recirculation of the hot gas suffices to maintain the distributed chemical reaction in a certain range of equivalence ratios before the flame fails, The reaction term may become small compared to the convection and conduction terms of the energy equation at the flame tip. leading to the non-monotonic curves in Fig. 4(a). The maximum value of W occurs at the tip when $Le_F = 1$ and away from the tip when $Le_F > 1$.

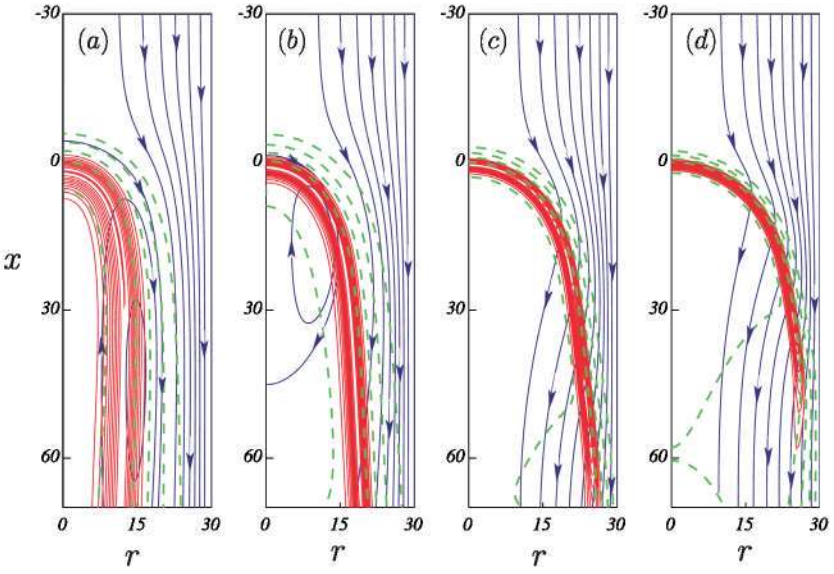

Fig. 6. Contours of constant reaction rate (solid, red), isotherms (dashed, green) and streamlines of the flow relative to the flame front (solid with arrows, blue) for $\phi = 0.421$ (*a*), 0.474 (*b*), 0.538 (*c*) and 0.581 (*d*). Here $R = 30$, $\Sigma = 0$, other parameters have their reference values. (For interpretation of the references to color in this figure legend, the reader is referred to the web version of this article.)

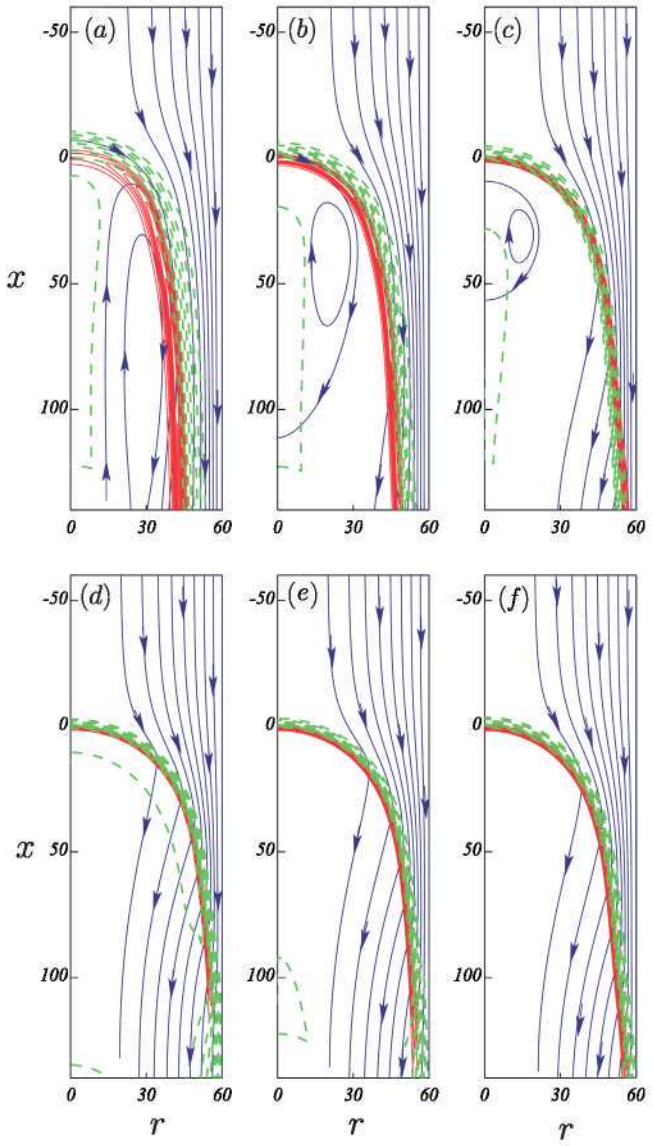

Fig. 7. Contours of constant reaction rate (solid, red), isotherms (dashed, green) and streamlines of the flow relative to the flame front (solid with arrows, blue) for flames with radiation losses ($\Sigma = 2 \times 10^{-5}$). Upper row: limit flames for (*a*): $Le_F = 0.8$ ($\phi_{lim} \approx 0.450$), (*b*): $Le_F = 1$ ($\phi_{lim} \approx 0.513$), and (*c*): $Le_F = 1.2$ ($\phi_{lim} \approx 0.556$). Lower row: flames for $\phi = 0.581$ and $Le_F = 0.8$ (*d*), 1 (*e*), and 1.2 (*f*). Other parameters have their reference values. (For interpretation of the references to color in this figure legend, the reader is referred to the web version of this article.)

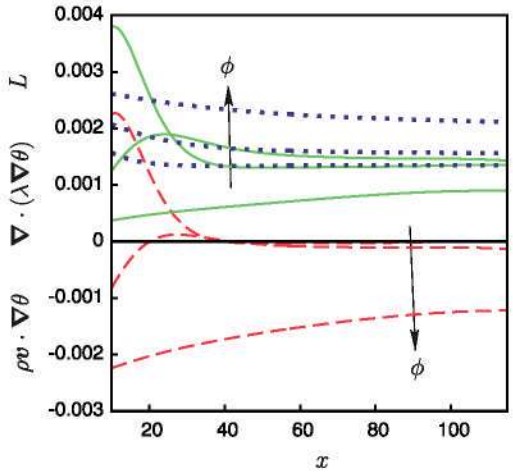

Fig. 8. Convection (dashed, red), conduction (solid, green) and radiation losses (dotted, blue) terms of the energy equation (5) in the burnt gas along the axis of the tube for $\phi = 0.513$, 0.527 and 0.581, increasing as indicated by the arrows. Other parameters have their reference values. (For interpretation of the references to color in this figure legend, the reader is referred to the web version of this article.)

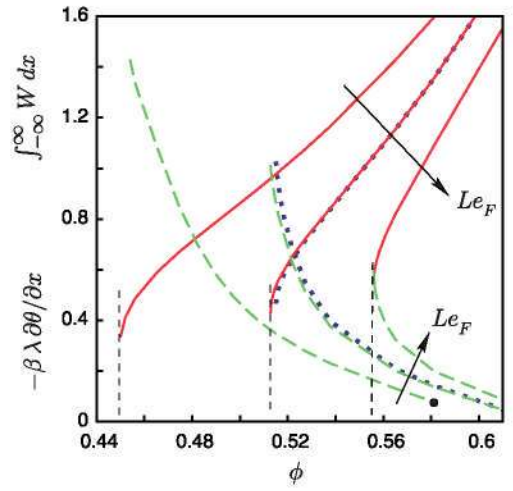

Fig. 9. Values at the axis of the tube of the reaction rate integrated across the flame, $\int_{-\infty}^{\infty} W\,dx$, (solid, red) and the scaled conduction flux toward the burnt gas, $-\beta\lambda\partial\theta/\partial x$ evaluated at the point where $W = 0.01\,W_{max}$ pass the maximum (dashed, green), as functions of the equivalence ratio for $Le_F = 0.8$, 1 and 1.2, increasing as indicated by the arrows. Other parameters have their reference values. Dotted curves show results for $Le_F = 1$ with the mass fractions of CO_2 and H_2O entering the expression of the Planck mean absorption coefficient computed separately with $Le_{CO_2} = 1.39$ and $Le_{H_2O} = 0.83$, as explained in Section 2. (For interpretation of the references to color in this figure legend, the reader is referred to the web version of this article.)

In any case, the results in Fig. 4(a) show that, in the absence of radiation losses, a flame exists for values of the equivalence ratio well below the experimental minimum measured in a standard flammability tube. On the other hand, analogous computations for $R = 30$ (a 26 mm diameter tube) fail to converge for $\phi_{lim} \approx 0.421$ when $Le_F = 1$, which is not far from the flammability limit measured by Shoshin et al. [10] in a 24 mm diameter tube; $\phi_{STJ} \approx 0.486$. This suggests that the results without radiation losses could be relevant for narrow tubes. The limit flame found in these computations for $R = 30$ is shown in Fig. 6(a).

3.2. Effect of the radiation losses

Figure 4(b) shows the same flame properties as Fig. 4(a) discussed above when radiation losses are taken into account with $\Sigma = 2 \times 10^{-5}$. As can be seen, radiation losses cause flame extinction at a value of ϕ that increases with the Lewis number of the fuel (from $\phi_{lim} \approx 0.450$ for $Le_F = 0.8$, to $\phi_{lim} \approx 0.513$ for $Le_F = 1$, and to $\phi_{lim} \approx 0.556$ for $Le_F = 1.2$) and is in the range of experimental values for lean limit methane/air flames measured in the standard flammability tube ($\phi_{exp} = 0.507$–0.517; see, e.g. Ref. [12]). Figure 7 shows the appearance of the limit flame fronts and the flow fields for the three values of Le_F, and compares them with less lean flame fronts with $\phi = 0.581$. Comparison of Figs. 7(e) and 3(d) shows that radiation losses have very little effect on the flame away from the flammability limit. However, the effect of radiation losses increases rapidly when the limit is approached. When $Le_F = 1.2$, Fig. 7(c), radiation-induced extinction occurs before the flame front can approach the recirculation region. In this case the tip of the flame is already weakened by the strain rate of the fresh gas flow, and radiation causes extinction with only a moderate decrease of the

equivalence ratio. When $Le_F = 0.8$, Fig. 7(a), the tip of the limit flame is around the dividing streamline. Now the strain rate of the fresh gas flow strengthens the flame, opposing the effect of radiation losses and postponing extinction to a smaller value of the equivalence ratio.

The important effect of radiation losses revealed by these computations is surprising, given the small value of Σ. The direct effect of the losses in the transport region of the flame leads to temperature variations of order $\Sigma(\gamma+1)^{3+\kappa}$ at most, and radiation losses would induce a dimensionless conduction flux of this same order immediately behind the flame, should the dimensionless mass flux ρu be of order unity downstream of the flame, as it is for a planar unstretched flame; see Williams [14] and Joulin and Clavin [24]. These perturbations are small compared to β^{-1} and therefore have little effect on the flame. This is in line with the results in Fig. 7(d)–(f) for $\phi = 0.581$. However, the decrease of the downward velocity of the gas and the eventual appearance of recirculation when the flammability limit is approached drastically enhances the effect of radiation losses.

Figure 8 shows the evolution along the axis of the tube of the convection (dotted), conduction (dashed) and radiation (solid) terms of the energy equation (5) in the burnt gas behind the flame for three values of the equivalence ratio. Conduction in the burnt gas is important and nearly balances radiation losses for the near limit flame with $\phi = 0.513$ (shown in Fig. 7(b)), but it is less important when $\phi = 0.581$ (flame shown in Fig. 7(e)), for which a convection–radiation balance is approached. The order of the radiation-induced temperature variation in the low velocity region of characteristic size R behind the near limit flame is $\Delta\theta \sim \Sigma(\gamma+1)^{3-\kappa}R^2$, from the conduction–radiation balance $\lambda\Delta\theta/R^2 \sim \rho\Sigma(\gamma+1)^4$ with $\rho \approx 1/(\gamma+1)$ and $\lambda \approx (\gamma+1)^\kappa$. The effect of this temperature variation on the reaction region of the flame is measured by the conduction flux it induces scaled with the inverse of the Zeldovich number (Williams [14], Joulin and Clavin [24]); $\beta\lambda_b\Delta\theta/R \sim \beta\Sigma(\gamma+1)^3R$, which is a quantity of order unity for $R = 60$ and typical values of the parameters involved.

To back up these estimates, Fig. 9 shows the values at the flame tip ($r = 0$) of the dimensionless heat released by the chemical reaction, $\int_{-\infty}^{\infty} W\,dx$ (solid), and the scaled conduction flux immediately behind the flame, $-\beta\lambda\partial\theta/\partial x$ (dashed), as functions of ϕ for $R = 60, \Sigma = 2\times10^{-5}$, and $Le_F = 0.8$, 1 and 1.2. This figure confirms that heat conduction toward the burnt gas due to radiation losses increases to significant values only in the vicinity of extinction. Direct radiation losses from the flame are small in any case.

Similar computations carried out for narrower tubes show that the effect of radiation losses decreases with R, in line with the estimations above. Thus, extinction occurs for $\phi_{lim} \approx 0.448$ when $R = 30$ and $Le_F = 1$, and the velocity of the gas is upward in the reaction region of the limit flame, which resembles the structure discussed in Section 3.1. This value of the limit equivalence ratio is to be compared to the value 0.421 computed in the absence of radiation losses, and to the value $\phi_{STP} = 0.486$ measured by Shoshin et al. [10] in a 24 mm diameter tube ($R = 27.9$).

4. Conclusions

The effect of radiation losses on very lean methane/air flames propagating upward in a vertical tube has been analyzed numerically using a simple model that comprises an optically thin gas and a single overall chemical reaction. Numerical results for the conditions of the standard flammability tube show that a region of low gas velocity relative to the flame, of characteristic size of the order of the radius of the tube, develops in the burnt gas when the equivalence ratio is decreased. Heat conduction is important in this region, despite its large size, and, in the presence of radiation losses, leads to a conduction heat flux from the flame to the burnt gas that causes extinction of the flame tip at a value of the equivalence ratio of the order of the experimental flammability limit. The velocity of the burnt gas increases, and radiation losses cease to play a significant role, when the equivalence ratio is increased.

The effect of the radiation losses decreases with the radius of the tube. Numerical results in the absence of radiation losses predict that a flame fails to propagate only when it is immersed in a region of reverse (upward) flow of the burnt gas that upsets the conduction–reaction balance in the flame reaction region. In the standard flammability tube, this would happen at values of the equivalence ratio well below the measured flammability limit. However, limit equivalence ratios computed without radiation losses for tubes narrower than the standard tube are in reasonable agreement with the flammability limit measured by Shoshin et al. [10] in a 24 mm diameter tube.

Acknowledgment

This work was supported through projects HYSYCOMB, S2009/ENE-1597 (Comunidad de Madrid) and CSD2010-00010 and DPI-20450-C03-01 (Ministerio de Economía y Competitividad).

References

[1] H.F. Coward, G.W. Jones, Limits of flammability of gases and vapors, U.S. Bureau of Mines Bull. #503, 1952.
[2] A. Levy, Proc. R. Soc. London A 283 (1965) 134–145.
[3] R.M. Davies, G.I. Taylor, Proc. R. Soc. London A 200 (1950) 375–390.
[4] V.S. Babkin, V.V. Zamashchikov, A.M. Badalyan, V.N. Krivulin, E.A. Kudryavtsev, A.N. Baraton, Fizika Goreniya i Vzryva 18 (1982) 4–52.
[5] B. Lewis, G. von Elbe, Combustion, Flames and Explosions of Gases, Academic Press, New York, 1961 (chap. 5).
[6] J. Jarosinski, R.A. Strehlow, A. Azarbarzin, Proc. Combust. Inst. 19 (1982) 1549–1557.
[7] M. Hertzberg, The theory of flammability limits: flow gradient effects and flame stretch, Bureau of Mines Report #8865, 1984.
[8] E. von Lavante, R.A. Strehlow, Combust. Flame 49 (1983) 123–140.
[9] F.J. Higuera, Combust. Flame 158 (2011) 885–892.
[10] Y.L. Shoshin, L. Tecce, J. Jarosinski, Combust. Sci. Technol. 180 (2008) 1812–1828.
[11] Y.L. Shoshin, J. Jarosinski, Proc. Combust. Inst. 32 (2009) 1043–1050.
[12] Y.L. Shoshin, G. Gorecki, J. Jarosinski, T. Fodemski, Combust. Flame 157 (2010) 884–892.
[13] M.D. Smooke, V. Giovangigli, in: M.D. Smooke (Ed.), Reduced Kinetic Mechanisms and Asymptotic Approximations for Methane–Air Flames, Lecture Notes in Physics, vol. 384, Springer, 1991, pp. 1–28.
[14] F.A. Williams, Combustion Theory, second ed., Benjamin Cummings, Menlo Park, CA, 1985 (chaps. 5, 8 and 10).
[15] S.G. Davis, J. Quinard, G. Searby, Combust. Flame 130 (2002) 130–136.
[16] I. Yamaoka, H. Tsuji, Proc. Combust. Inst. 20 (1984) 1883–1892.
[17] S.-F. Wang, H. Zhang, J. Jarosinski, A. Gorczakowski, J. Podfilipski, Combust. Flame 157 (2010) 667–675.
[18] C.K. Westbrook, F.L. Dryer, Combust. Sci. Technol. 27 (1981) 31–43.
[19] J.R. Howell, R. Siegel, M.P. Menguc, Thermal Radiation Heat Transfer, fifth ed., CRC Press, Boca Raton, FL, 2011 (chaps. 9 and 10).
[20] Y. Ju, H. Guo, F. Liu, K. Maruta, J. Fluid Mech. 379 (1999) 165–190.
[21] W.A. Fiveland, ASME J. Heat Transf. 106 (1984) 699–706.
[22] A. Soufiani, J. Taine, Int. J. Heat Mass Transf. 40 (1997) 987–991.
[23] J. Buckmaster, D. Mikolaitis, Combust. Flame 45 (1982) 109–119.
[24] G. Joulin, P. Clavin, Acta Astronaut. 3 (1976) 223–240.